Positive and negative pull-back instabilities in mode splitting optomechanical devices

Hailong Pi,[1] Carlo Edoardo Campanella,[2]* David J. Thomson,[3] Jize Yan[1]*

[1]School of Electronics and Computer Science, University of Southampton, Southampton SO17 1BJ, United Kingdom.

[2]QOpSys s.r.l., 70023 Bari, Italy.

[3]Optoelectronics Research Centre, University of Southampton, Southampton SO17 1BJ, United Kingdom.

*Corresponding Authors: ce.campanella@qopsys.com, J.Yan@soton.ac.uk

Abstract

Optical gradient forces play an essential role in optomechanical systems. The systems based on coupled microresonators are of great importance for applications in signal processing, sensors and actuators. Here, we theoretically and experimentally studied, for the first time, positive and negative pull-back instabilities originating from attractive and repulsive optical gradient forces, respectively, in an optomechanical device based on coupled microrings. The device consists of two coupled free-standing waveguides in two identical microrings, fabricated in the silicon-on-insulator process. The coupling between the two microrings results in the symmetric and antisymmetric resonances showing in the transmission spectrum of the device. By measuring the wavelength difference between the self-reference symmetric and antisymmetric resonances, the wavelength tuning due to the optomechanical actuation is decoupled from the tuning due to the thermo-optical effect. It is demonstrated theoretically and experimentally that the positive pull-back instability originates from the attractive optical gradient force and the negative pull-back instability originates from the repulsive optical gradient force when the pump wavelength increases. The positive pull-back instability significantly increases the wavelength difference between the symmetric and antisymmetric resonances. On the contrary, the negative pull-back instability significantly decreases the wavelength difference.

Keywords: pull-back instability, optomechanics, optical gradient force, coupled microresonators, mode splitting

Table of Contents Graphic

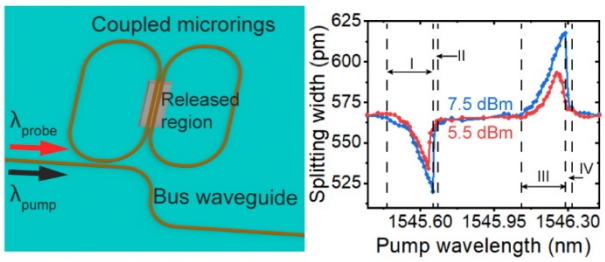

Introduction

Micro- and nano-optomechanical systems have been widely investigated for optical signal processing,[1-3] sensors[4-6] and actuators.[7-9] Optical gradient forces play an essential role in the systems and originate from the gradient of the electromagnetic field in the near-field of the guided wave structures.[10] The strong field gradient leads to strong optical gradient forces. Microresonators with high quality (Q) factor and small mode volume have been widely utilized in optomechanical systems to enhance optical gradient forces.[11-13]

In the presence of strong coupling between two identical microresonators, the symmetry and degeneracy of the resonator modes are broken, and symmetric (S) and antisymmetric (AS) resonant modes emerge.[14] Based on the coupled microrings, the optical gradient force in optomechanical systems can be attractive or repulsive by pumping different resonant modes.[1, 15, 16] The attractive and repulsive optical forces offer a flexible way to drive nano-scale mechanical structures. Meanwhile, the displacement of the nanostructures can be detected by self-referenced S and AS resonances.[17] Based on the actuation flexibility and displacement detection by utilizing S and AS resonances, potential applications of all-optical reconfigurable photonic circuits have been demonstrated.[1, 17, 18]

Ref. 9 reports a nano-optomechanical actuator that consists of a single microring resonator with pull-back instability (PBI) that arises from the nonlinear attractive optical gradient force on a deflected waveguide. PBI means that a small variation of initial conditions results in a significant change in the deflection of nanostructures, and the structures are pulled back towards their initial positions.[9] The PBI can cause a significant resonance shift and has potential applications for optomechanical memory,[19] optical switches[20] and on-chip optical diode.[13, 21] However, the PBI arising from the attractive and repulsive optical gradient forces in a coupled-resonator optomechanical system has not been investigated.

This paper theoretically and experimentally studied the PBIs of a nano-optomechanical device driven by attractive and repulsive optical gradient forces generated by pumping the S and AS optical modes, respectively. The wavelength tuning due to optical gradient forces is recognized by the intrinsic self-referenced S and AS resonances. It is demonstrated that the attractive and repulsive optical gradient forces induce two counter-directional PBIs, named positive and negative PBIs. The positive PBI (pPBI) causes a significant increase in the wavelength difference between the S and AS resonances. On the contrary, the negative PBI (nPBI) causes a substantial decrease in the wavelength difference. The demonstrated PBIs, together with the intrinsic self-referenced detection scheme based on S and AS resonances, could be useful for optical information processing and offer an ultrasensitive platform of optomechanical sensors.

The paper is structured as follows. The first section describes the structure of the optomechanical device. In the second section, the optical gradient forces are calculated, and PBIs are theoretically studied. To demonstrate the PBIs, the fabricated optomechanical device and the experimental setup are presented in the next section. Finally, the PBIs are demonstrated based on shifts of S and AS resonances and the wavelength difference between the S and AS resonances, verifying the theoretical analysis in the second section.

Optomechanical device based on two coupled microresonators

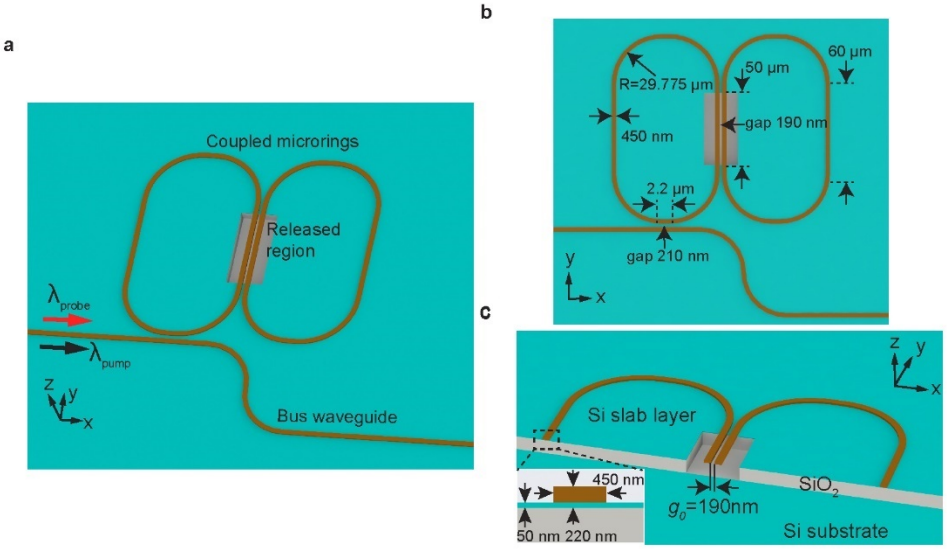

Fig. 1. (a) The schematic of the optomechanical device contains two laterally coupled microrings and a bus waveguide. Each microring has a free-standing waveguide. The pump light generates optical gradient forces. The probe light detects resonance shifts of the device. (b) Top view of the device. The dimensions of the device are specified. (c) The cross-sectional view of the device. The dimensions of the rib waveguide are shown in the inset.

This paper demonstrated an optomechanical device to study the PBI effects. The device provides a simple actuation scheme for tuning optical resonance, which is useful for optical information processing, such as optical filters. The device consists of two free-standing waveguides in two identical racetrack microrings and a bus waveguide, as shown in Fig. 1. Each microring has a free-standing waveguide with a length of 50 μm. An air gap between the two suspended waveguides is 190 nm. The air gap between the suspended waveguide and the substrate is about 1.6 μm. The height and width of the suspended waveguides are 220 nm and 450 nm, respectively. Outside the released regions, the waveguides are rib waveguides and have the same cross-section with an overall height of 220 nm, a waveguide width of 450 nm, and an etch depth of 170 nm. The thickness of the Si slab layer is 50 nm.

The rib waveguides are used to prevent hydrofluoric acid (HF) vapour etching of the SiO_2 layer outside the released region when releasing the suspended waveguides. The bending radius of the microrings is 30 μm, defined from the middle of the waveguides. The coupling gap between the bus waveguide and the left ring is 210 nm. The coupling length is 2.2 μm for the coupling between the bus waveguide and the left microring.

Calculation of optical gradient forces and resonance shifts of the device

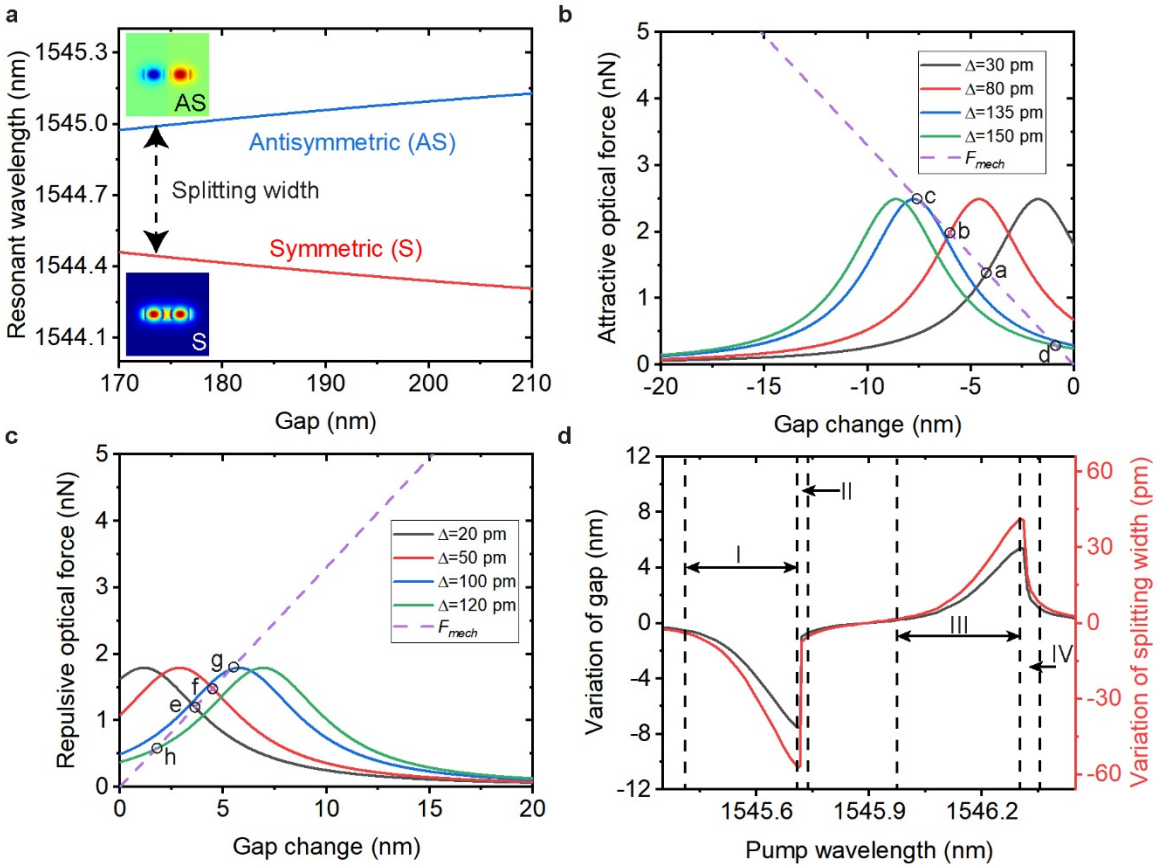

Fig. 2. (a) Simulated variations of the S and AS resonances as the air gap between two suspended waveguides is changed. The coupling between the two microrings is so strong that the wavelength splitting spans more than one free spectral range of the device. So the two neighbouring modes (S and AS modes) shown in the figure have different azimuthal orders. The insets show the electric field profiles for the S and AS modes. (b) Comparison of the simulated mechanical force and attractive optical gradient force. $\Delta = \lambda_{in}$-1545.58 nm. 1545.58 nm is the measured S resonance (λ_{r0}^{+}). (c) Comparison of the simulated mechanical force and repulsive optical gradient force. $\Delta = \lambda_{in}$-1546.21 nm. 1546.21 nm is the measured AS resonance (λ_{r0}^{-}). (d) Simulated nonlinear variations of the air gap between the two suspended waveguides. The pump laser wavelength increases from 1545.35 nm to 1546.45 nm. The range (1545.35-1546.45 nm) covers an S resonance (λ_{r0}^{+}=1545.58 nm) and an AS resonance (λ_{r0}^{-}=1546.21 nm). The simulated nonlinear

changes of the splitting width between the S (λ_{r0}^{+}) and AS (λ_{r0}^{-}) resonances are also presented.

In this section, the PBI of the optomechanical device will be theoretically analyzed. The two microrings of the designed device are identical and coupled. The degeneracy of the resonator modes is broken, and the mode pairs (S and AS modes) appear.[14, 16] Figure 2(a) shows the S and AS resonances with the air gap between the two suspended waveguides. The insets show the electric field profiles for the S and AS modes. The S and AS resonances depend on the gap of the two rings. The difference between the two resonant wavelengths is defined as the splitting width, which increases when the gap increases. Strictly speaking, the splitting width is the wavelength difference between the S and AS resonances with the same azimuthal order. Here, we use the splitting width to present the wavelength difference between two neighbouring modes without considering the requirement of the same azimuthal order. It is worth noting that the two neighbouring modes shown in Fig. 2(a) have different azimuthal orders due to the strong coupling causing the splitting spanning more than one free spectral range of the device. The calculated resonances shown in Fig 2(a) are obtained from the device's transfer function that is calculated based on two coupling matrices.[22] One is the coupling matrix to represent the coupling between the bus waveguide and the left microring.[23] Another matrix represents the coupling between the two microrings and is calculated based on the coupled-mode theory in space.[24, 25] The coupling coefficient K between the two microrings can be calculated using the effective indices of the S and AS modes. $K = \pi/\lambda \cdot (n_+ - n_-)$.[16, 26] The effective index of the S mode corresponds to n_+, and the AS mode is n_-. The effective indices are calculated using a finite-difference eigenmode (FDE) solver (Lumerical MODE Solutions).

The optical energy will be stored in the microrings when the device is pumped. The optical gradient forces can be derived from the relation between the stored optical energy and the gap[9, 27]

$$F_{opt}^{\pm} = -\frac{\partial U^{\pm}}{\partial g} = \frac{2(\tau_e^{\pm})^{-1}P_{in}}{(\lambda_{in}-\lambda_r^{\pm})^2(2\pi c)^2(\lambda_r^{\pm})^{-3}+\lambda_r^{\pm}((\tau_i^{\pm})^{-1}+(\tau_e^{\pm})^{-1})^2}\frac{\partial \lambda_r^{\pm}}{\partial g} \quad (1)$$

where U is the optical energy stored in microrings, ∂g represents the variation of the gap when the two suspended waveguides bend. The gap is between the midpoints of the two suspended waveguides. P_{in} is the power of the control light in the bus waveguide, λ_{in} is the wavelength of the control light, λ_r is the resonant wavelength, τ_i is the decay rate due to the internal loss, τ_e is the decay rate due to the coupling between the microring and the bus waveguide, $\partial\lambda_r/\partial g$ is the optomechanical tuning efficiency. The superscript ± stands for either the S (+) or AS (-) optical mode.

The resonant wavelengths in Eq. (1) are given by

$$\lambda_r^{\pm} = \lambda_{r0}^{\pm} + \delta\lambda_{om}^{\pm} + \delta\lambda_{to}^{\pm} \quad (2)$$

where λ_{r0} is the unshifted resonant wavelength, $\delta\lambda_{om}$ is the resonance shift due to the optomechanical actuation. $\delta\lambda_{to}$ is the resonance shift induced by the thermo-optical effect. The resonance shift due to the optomechanical actuation can be written as

$$\delta\lambda_{om}^{\pm} = \Delta g \cdot \partial\lambda_r^{\pm}/\partial g \quad (3)$$

where Δg is the change of the gap due to the optical gradient force. The gap is between the midpoints of the two suspended waveguides. The resonance shift due to the thermo-optical effect can be expressed as[28-30]

$$\delta\lambda_{to}^{\pm} = \lambda_{r0}^{\pm}/n_g \cdot k_{th}\Delta T \quad (4)$$

where n_g is the group index, and k_{th}=1.86×10^{-4} K^{-1} is the silicon thermo-optic coefficient. ΔT is the steady-state temperature change in the microrings. It can be expressed as[1, 31] $\Delta T=\Gamma_{abs}R_{th}U^{\pm}$, where Γ_{abs} is the total optical absorption rate, R_{th} is the thermal resistance of the microrings.

The optomechanical tuning coefficient $\partial\lambda_r/\partial g$ in Eq. (1) can be obtained from Fig. 2(a). In the device, the initial gap is 190 nm, $\partial\lambda_r^{\pm}/\partial g = \mp 3.8 \times 10^{-3}$. Based on Eq. (1), pumping the S mode can generate the attractive optical gradient force that pulls the two suspended waveguides towards each other. On the contrary, pumping the AS mode can generate the repulsive optical gradient force that pushes the two waveguides away from each other.

The deflection of the two waveguides gives rise to a mechanical force $F_{mech}=k_{mech}\cdot\Delta g/2$. k_{mech} is the spring constant of a suspended waveguide. The mechanical spring constant is simulated to be 0.66 N/m using finite-element analysis (FEA) software COMSOL. Compared to the optical gradient forces, the mechanical force tends to pull the waveguides to their original positions. The optical force and the mechanical force balance each other at the equilibrium point,

$$F_{opt}(\Delta g) + k_{mech} \cdot \Delta g/2 = 0 \quad (5)$$

The balances between the mechanical forces and the optical gradient forces are numerically analyzed. The pump power in the simulation is P_{in}=7.5 dBm. The parameters for calculating the stored energy U are obtained by fitting the notches of S and AS modes in the measured transmission spectrum with the device's transfer function derived from the time-domain coupled-mode analysis.[32, 33] The transmission spectrum is described in the sections of Experimental Results. The air gap between the two suspended waveguides is 190 nm. For the S mode, the resonant wavelength is λ_{r0}^{+}=1545.58 nm, the intrinsic Q factor of the coupled microrings is $Q_i=\omega_{r0}^{+}\tau_i/2$=35310, and the Q factor for the waveguide-resonator coupling is $Q_e=\omega_{r0}^{+}\tau_e/2$=28660. For the AS mode, the resonant wavelength is λ_{r0}^{-}=1546.21 nm, the intrinsic Q factor of the coupled microrings is $Q_i=\omega_{r0}^{-}\tau_i/2$=25120, and the Q factor for the waveguide-resonator coupling is $Q_e=\omega_{r0}^{-}\tau_e/2$=25120. The thermal resistance between the coupled microrings and

the surroundings is R_{th}=7625 K/W, calculated using FEA software COMSOL.[13] The optical absorption rate Γ_{abs} is estimated using the absorption limited quality factor $Q_{abs}=\omega/\Gamma_{abs}$,[1] where $Q_{abs}=10^6$.[17, 34]

Figure 2(b) shows the balance between the mechanical force and the attractive optical gradient force. The detuning Δ is defined as the difference between the pump laser wavelength and the unshifted S resonance λ_{r0}^{+}=1545.58 nm. Δ= λ_{in}-1545.58 nm. The gap change in Fig. 2 means the change in the gap between the midpoints of the two suspended waveguides when the waveguides are deflected from their initial positions. The initial gap is 190 nm. When Δ increases, the equilibrium point changes from point a to point c, and the gap decreases with the pump laser wavelength. It is because the pump laser approaches the S resonance (λ_r^{+}), more power is stored in the microrings, increasing the generated attractive force. At point c, the deflection is the largest. This means the pump laser wavelength is the same as the S resonance λ_r^{+}. When Δ increases, the equilibrium point changes from point c to d. The gap significantly increases, and the suspended waveguides are pulled back towards the initial positions. This phenomenon is called PBI.[9] We name it pPBI to distinguish it from the one caused by the repulsive optical gradient force.

Figure 2(c) shows the balance between the repulsive optical gradient force and the mechanical force. The detuning is defined as the difference between the pump laser wavelength and the unshifted AS resonance λ_{r0}^{-}=1546.21 nm. Δ= λ_{in}-1546.21 nm. It is observed that the gap increases with the pump laser wavelength when the equilibrium point changes from e to g. At point g, the gap is the largest. When Δ increases, the equilibrium point changes from g to h. The gap decreases significantly, and the two suspended waveguides are pulled back towards their initial positions. Here, we use nPBI to describe the significant decrease of the gap.

Figure 2(d) presents the nonlinear variation of the gap as the pump wavelength increases from 1545.35 nm to 1546.45 nm. The range of the pump laser wavelength covers an S resonance (λ_{r0}^{+}=1545.58 nm) and an AS resonance (λ_{r0}^{-}=1546.21 nm). It is observed that there are four main changes (Indicated using regions I, II, II and IV) of the gap. Regions I and II show that the gap changes when the S mode is pumped. In region I, The gap decreases when the pump wavelength increases. In region II, a small increase in the pump laser wavelength induces a significant increase in the gap, indicating the occurrence of pPBI. Regions III and IV show that the gap changes when the AS mode is pumped. In region III, the gap increases with the pump laser wavelength. In region IV, a significant decrease in the gap is caused by a small increase in the pump laser wavelength, showing the occurrence of the nPBI.

According to Fig. 2(a), the variation of the gap shown in Fig 2(d) gives rise to changes in the splitting width. Figure 2(d) also shows the nonlinear changes of the splitting width when the pump wavelength increases.

Fabricated device and experimental setup

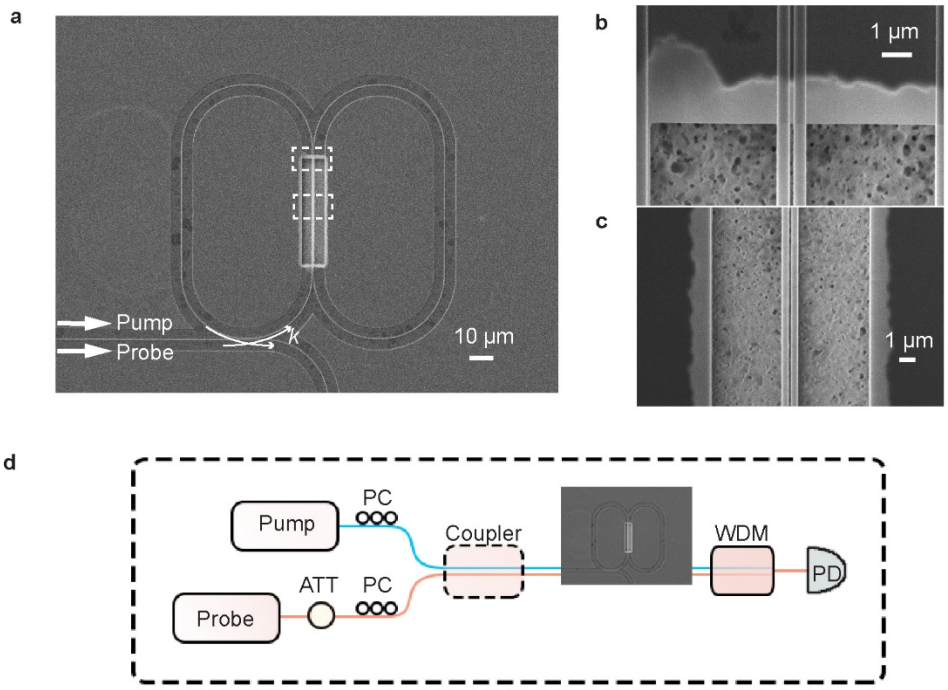

Fig. 3. (a) SEM image of the fabricated nano-optomechanical device. This device includes two coupled microrings and a bus waveguide. Each microring has a free-standing waveguide. The two dashed rectangles indicate the regions shown in (b) and (c). (b) SEM image of the connections between the rib waveguides and the suspended waveguides. (c) SEM image of the centre region of the suspended waveguides. (d) Schematic of the experimental setup. The pump light is used to control optical forces, and the probe light is used to read out shifts of the device's resonances. The pump and probe are coupled using an optical coupler and launched into the bus waveguide. A wavelength division multiplexer is used to filter the pump light. The optical transmission spectrum is obtained from the photodetector that is synchronized with the probe light source.

The optomechanical device shown in Fig. 1 is fabricated in a silicon-on-insulator (SOI) process to demonstrate the PBIs induced by the attractive and repulsive optical gradient forces. Figure 3(a) shows an SEM image of the fabricated device. Details of the fabrication process are described in the section of Methods. In the coupling region between the bus waveguide and the left microring, two arrows in Fig. 3(a) show that light couples in and out of the microring with the power coupling efficiency *k*. The efficiency is 27% when the wavelength is 1545.58 nm. The dashed rectangles indicate the regions

shown in Fig. 3(b)(c). Figure 3(b) shows the connections between the suspended waveguides and the rib waveguides. Figure 3(c) shows the central region of the two coupled suspended waveguides.

Figure 3(d) illustrates the schematic of the experimental setup used to measure the transmission spectra of the coupled microrings. The pump laser is high-power and utilized to induce optical gradient forces to deflect the two suspended waveguides. The low-power probe laser sweeps in wavelength to read out the resonance shift of the device. An attenuator (ATT) is used to reduce the power of the probe laser. A polarization controller (PC) is used after each laser to excite transverse electric mode in the device. The pump and probe are coupled using an optical coupler (OC) and launched into the bus waveguide. The output pump and probe are separated by a wavelength division multiplexer (WDM). A photodetector (PD) is synchronized with the probe laser to record the probe transmission.

Experimental results

Shifts of split resonances when the device is pumped

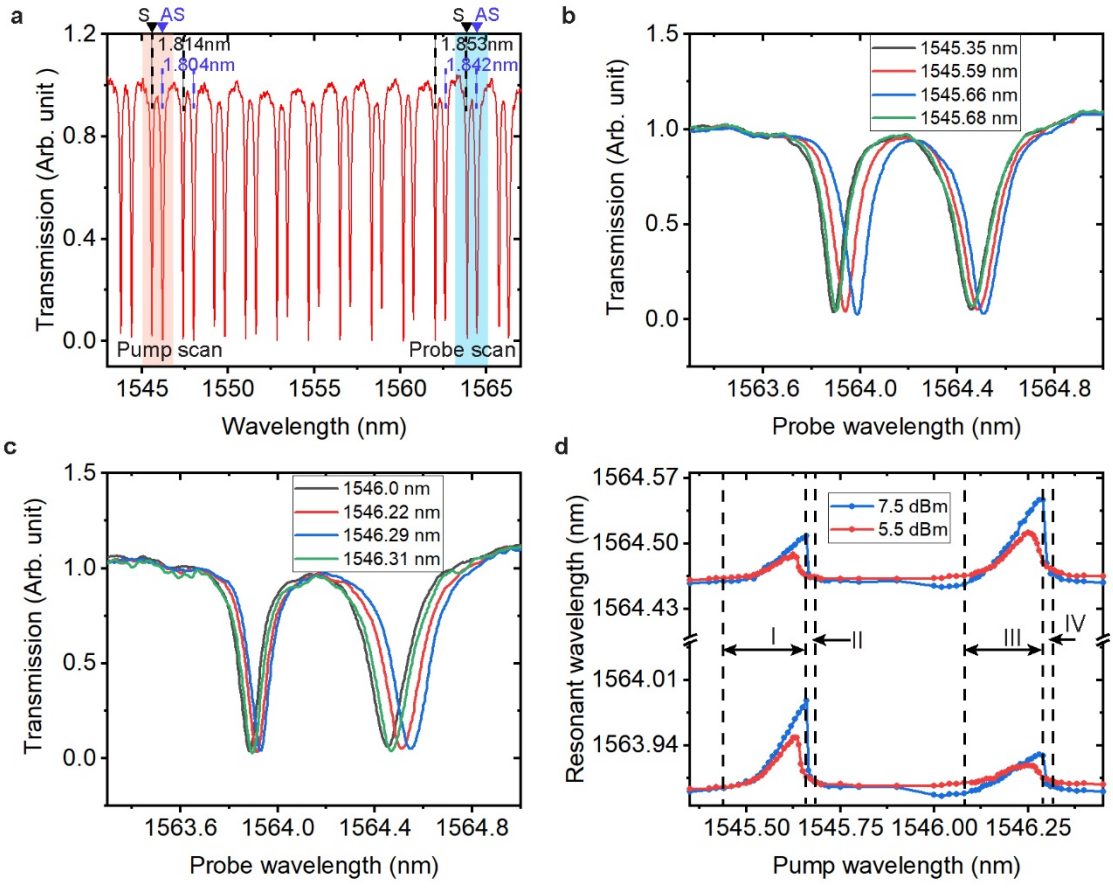

Fig. 4. (a) The transmission spectrum when only the probe light is used. The orange region highlights the pump scan region (1545.35-1546.45 nm). The blue region (1563.3-1565 nm) highlights the probe scan region. (b) Measured transmission spectra when the pump laser

wavelength increases and pumps the left notch in the pump region. (c) Measured transmission spectra when the pump laser wavelength increases and pumps the right notch in the pump region. (d) Shifts of the S and AS resonances in the probe scan region when the pump laser wavelength increases in the pump scan region.

Figure 4(a) presents the transmission spectrum of the device using the probe laser in the bus waveguide. The split notches in the transmission indicate the occurrence of mode splitting. The S and AS modes can be identified based on the free-spectral range (FSR).[1] The measured FSRs for the split modes are shown in Fig. 4 (a). The FSR for the left mode in the pump scan region (Orange region) is 1.814 nm, and the FSR for the right mode in the region is 1.804 nm. The larger FSR indicates that the left mode in the region is S mode and the right mode in the region is AS mode. The theoretical values of the FSRs of the S (1545.58 nm) and AS (1546.21 nm) resonances are 1.800 nm and 1.790 nm, respectively,[35] matching well with the FSRs obtained directly from Fig. 4(a). For the two modes in the probe scan region (Blue region), the left mode with the FSR of 1.853 nm is recognized as the S mode. The right mode with the FSR of 1.842 nm is the AS mode. In the experiments, the pump wavelength is increased in the pump scan region and induces optical gradient forces. In the probe scan region, the probe transmission is recorded to measure the resonance shifts.

Pumping the device will induce the optomechanical actuation and thermo-optical effect. The S and AS resonances will be shifted by the two effects. The optomechanical actuation changes the gap between the two microrings. The optical coupling coefficient between the two microrings depends exponentially on the gap. According to Fig. 2(a), increasing the gap will blue shift the S mode and red-shift the AS modes while decreasing the gap will red-shift the S mode and blue-shift the AS mode. For the shifts of the S and AS resonances due to the thermo-optical effect, their ratio can be calculated based on Eq. (4). The ratio is $\delta\lambda_{to}^{+}/\delta\lambda_{to}^{-} = (\lambda_{r0}^{+}/n_g^{+})/(\lambda_{r0}^{-}/n_g^{-}) = 1$, where λ_{r0}^{+}=1545.58 nm, λ_{r0}^{-}=1546.21 nm. n_g^{+}/n_g^{-} is calculated based on the FSRs (1.814 nm for the S mode and 1.804 nm for the AS resonances).[35] The ratio of 1 means that the thermo-optical effect leads to the same shifts of the S and AS resonances.

In Fig. 4(b), the S mode in the pump scan region is pumped. The transmission with pump laser wavelength of 1545.35 nm is for reference as no pump power drops into the microrings. When the pump laser wavelength changes by 310 pm from 1545.35 nm to 1545.66 nm, It is measured that the S resonance is red-shifted by 97 pm, and the AS resonance is red-shifted by 51 pm. The red-shifts of the S and AS resonances indicate that the thermo-optical effect dominates the wavelength tuning. If the optomechanical actuation dominates, one resonance will be red-shifted, and another will be blue-shifted. It is also observed that the S resonance has a larger shift compared to the AS resonance. This is because the attractive optical gradient force is induced by pumping the S mode in the pump scan region, decreasing the gap between two microrings and causing the red-shift of the S resonance and the blue-

shift of the AS resonance. When the pump laser wavelength increases by 20 pm from 1545.66 nm to 1545.68 nm, both the S and AS resonances experience significant decreases. When the pump laser wavelength is 1545.68 nm, the resonances in the probe scan region are very close to the reference resonances with no pump power dropping into the microrings. This means the two suspended waveguides are almost pulled back to their initial positions, and the pPBI occurs.

In Fig. 4(c), the AS mode in the pump scan region is pumped. The transmission with pump laser wavelength of 1546 nm is for reference as no pump power drops into the microrings. When the pump laser wavelength increases from 1546 nm to 1546.29 nm, both the S and AS resonances are red-shifted, indicating that the thermo-optical effect dominates the wavelength tuning. Compared to the S resonance, the AS resonance has a larger wavelength shift. This is because the repulsive optical gradient force increases the gap between the microrings. When the pump laser wavelength increases from 1546.29 nm to 1546.31 nm, the S and AS resonances experience significant decreases and are close to the reference resonances. This indicates the occurrence of the nPBI.

Figure 4(d) summarises the shifts of the S and AS resonances in the probe scan region. The pump laser wavelength increases in the pump scan region from 1545.35 nm to 1546.45 nm. The measurement is carried out with the pump power of 7.5 dBm and 5.5 dBm, respectively. It is observed that each resonance experiences four main changes. Regions I, II, III and IV are shown to present the four changes when the pump power is 7.5 dBm. Regions I and II show the shifts of the S and AS resonances when the S mode in the pump scan region is pumped. The significant change of the resonances in region II is due to pPBI. Regions III and IV present the shifts of the S and AS resonances when the AS mode in the pump scan region is pumped. The significant change of the resonances in region IV is due to nPBI.

Variation of mode splitting width when the device is pumped

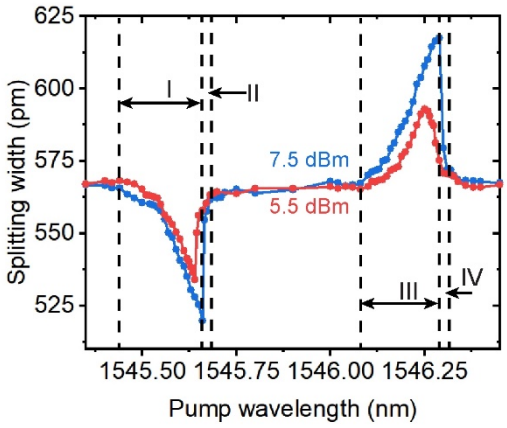

Fig. 5. Measured splitting width between the S and AS resonances in the probe scan region. The pump wavelength is increased in the pump scan region.

The shifts of split resonances shown in Fig 4(d) result from the optomechanical actuation and the thermo-optical effect. It is necessary to decouple the thermo-optical effect in order to obtain the wavelength tuning due to optomechanical actuation. As discussed above, the thermo-optical effect leads to the same shifts of the S and AS resonances. Therefore, the variation of the splitting width between the S and AS resonances presents the contribution from optomechanical actuation. Figure 5 shows the measured variations of the splitting width between the S and AS resonances in the probe scan region. The pump laser wavelength increases in the pump scan region from 1545.35 nm to 1546.45 nm.

The splitting width experiences four main changes when the pump laser wavelength increases. Regions I, II, III and IV are plotted to present the four changes when the pump power is 7.5 dBm. The regions are the same as the regions in Fig 4(d). It clearly shows that the splitting width experiences a significant increase in region II where the pPBI occurs, and a significant decrease in region IV where the nPBI occurs. It can also be observed that the difference between the blue (7.5 dBm) and red (5.5 dBm) lines changes nonlinearly with the pump wavelength. The significant differences appear in regions II and IV where the PBIs occur.

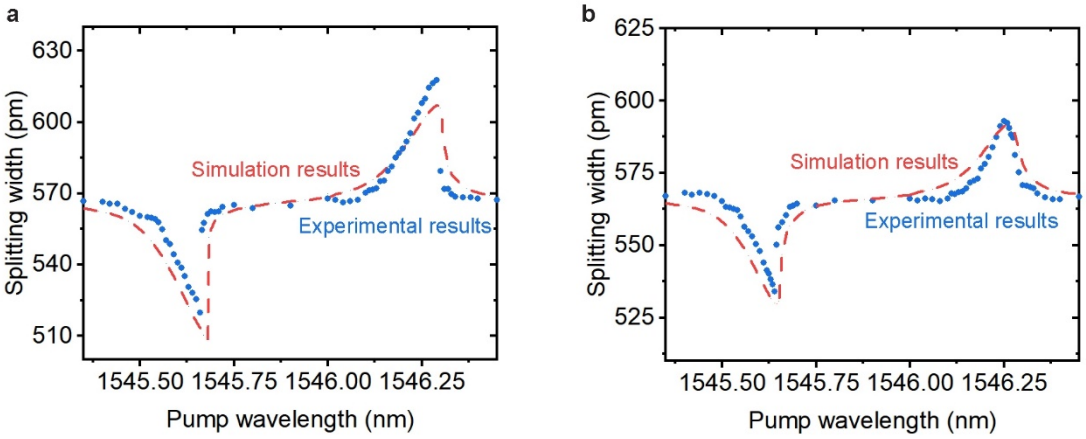

Fig. 6. (a) Comparison between the simulation and experimental results of the splitting width. The splitting width is between the S and AS resonances in the probe scan region. The pump power is 7.5 dBm, and the pump wavelength is increased in the pump scan region. (b) Comparison between the simulation and experimental results of the splitting width when the pump power is 5.5 dBm.

Figure 6 shows the simulation and experimental results of the mode splitting width between the S and AS resonances. The pump power is 7.5 dBm in Fig. 6(a) and is 5.5 dBm in Fig. 6(b). In the simulation, the absorption limited quality factors, Q_{abs}=1.4×10^6 for the S mode and 1.2×10^6 for the AS mode, are used to fit the experimental results. Figure 6 shows that the simulation results agree well with the experimental results, which verifies the theoretical analysis of PBIs.

Discussion

The pPBI and nPBI have been theoretically and experimentally studied in an optomechanical device based on two coupled microrings. The pPBI originates from the attractive optical gradient force generated by pumping the S optical mode. The occurrence of pPBI induces a significant increase in the splitting width between the S and AS resonances. On the contrary, the nPBI originates from the repulsive optical gradient force generated by pumping the AS optical mode. The nPBI induces a significant decrease in the splitting width.

The PBIs are physically similar to the optomechanical buckling transitions.[36] The stable positions of moveable nanostructures in the optomechanical systems are determined by the points where the optical forces balance the mechanical force. When the PBIs or the buckling transitions occur, the positions of the nanostructures experience significant changes. The PBIs will pull the nanostructures back towards their initial positions. On the contrary, the buckling transitions push the nanostructures away from their initial positions.

Experimental results in Fig. 4 show that the shifts of the S and AS resonances are due to the optomechanical-tuning effect and the thermal effect. The two effects could provide a new degree of freedom for designing all-optical photonic devices for optical information processing. The optomechanical-tuning effect can be adjusted by changing the dimensions of the suspended waveguides or the gap between them. When the wavelength tuning due to the optomechanical actuation is balanced by the tuning due to the thermal effect, the S and AS resonances can be controlled individually. The selective control can benefit the reconfigurable optical filter and optical router.

Figure 5 shows the significant changes of the mode splitting width when PBIs occur. The changes can be utilized for ultra-sensitive sensing. For example, it can be used to measure the variations in the refractive index of the coupled microrings. The variations cause the resonance shift and induce the PBIs. The information of variations can be extracted from the significant change in the splitting width between S and AS resonances.

Conclusion

We have demonstrated an on-chip optomechanical device based on two coupled microring resonators. The coupled resonators possess positive and negative PBIs originating from the attractive and repulsive optical gradient forces, respectively. By measuring the splitting width between the self-referenced S and AS resonances, the wavelength tuning by optomechanical actuation is decoupled from the tuning by the thermo-optical effect. The splitting width experiences a significant increase when the pPBI occurs and experiences a significant decrease when the nPBI occurs. The nonlinear changes of the splitting width are studied by combining the numerical calculation and experimental results.

The optomechanical actuation and thermo-optical effect of the Si optomechanical device can be used to design all-optical photonic devices for optical information processing, such as optical filters. The device can also be utilized for ultrasensitive sensing, based on the significant change of the mode splitting width induced by the PBIs. The design can be further explored for achieving phonon lasing,[37, 38] light delaying,[39, 40] exceptional points in parity-time symmetric systems[41, 42] or extending the mode localization effects from MEMS coupled resonant sensors[43] to the optomechanical domain to achieve ultrasensitive optomechanical mode-localized sensors.

Methods

Device fabrication

The device was fabricated on an SOI wafer with a 220-nm-thick device layer and a 2-μm buried oxide layer. A 40-nm-thick silicon dioxide layer was deposited by plasma-enhanced chemical vapour deposition (PECVD) as a hard mask to ensure the waveguide has a good profile and reduce optical loss. The bus waveguide and two coupled microrings are patterned using electron beam lithography (EBL) and inductively coupled plasma (ICP) etching of 170 nm into the Si device layer. A second EBL step followed by shallow ICP etching of 70 nm into the Si device layer is used to pattern the grating couplers. Then the strip waveguides contained in two coupled microrings were patterned using EBL and additional ICP etching of 50 nm Si device layer. Finally, HF vapour etching is utilized to release the free-standing waveguides from the substrate.

Author contributions

J. Y. and C. E. C. conceived and supervised the research; H. P. designed and fabricated the devices and performed the measurement; D. J. T. helped in the fabrication and measurement. All authors discussed the results and contributed to writing this manuscript.

Notes

The authors declare no competing financial interest.

Funding Sources

The research has been partially supported by EPSRC (EP/V000624/1) and PhD funding support from QOpSys SRL.

Acknowledgments

D. J. Thomson acknowledges funding from the Royal Society for his University Research Fellowship. We thank K. Kiang, Y. Feng and X.M. Xu (University of Southampton) for their help in fabrication and measurement.

References

(1) Wiederhecker, G. S.; Chen, L.; Gondarenko, A.; Lipson, M., Controlling Photonic Structures Using Optical Forces. *Nature* **2009,** *462*, 633-636.

(2) Rosenberg, J.; Lin, Q.; Painter, O., Static and Dynamic Wavelength Routing Via the Gradient Optical Force. *Nat. Photonics* **2009,** *3*, 478-483.

(3) Huang, J.; Chin, L. K.; Cai, H.; Li, H.; Wu, J. H.; Chen, T.; Li, M.; Liu, A.-Q., Dynamic Phonon Manipulation by Optomechanically Induced Strong Coupling between Two Distinct Mechanical Resonators. *ACS Photonics* **2019,** *6*, 1855-1862.

(4) Eichenfield, M.; Camacho, R.; Chan, J.; Vahala, K. J.; Painter, O., A Picogram- and Nanometre-Scale Photonic-Crystal Optomechanical Cavity. *Nature* **2009,** *459*, 550-555.

(5) Anetsberger, G.; Arcizet, O.; Unterreithmeier, Q. P.; Rivière, R.; Schliesser, A.; Weig, E. M.; Kotthaus, J. P.; Kippenberg, T. J., Near-Field Cavity Optomechanics with Nanomechanical Oscillators. *Nat. Phys.* **2009,** *5*, 909-914.

(6) Pruessner, M. W.; Park, D.; Stievater, T. H.; Kozak, D. A.; Rabinovich, W. S., Optomechanical Cavities for All-Optical Photothermal Sensing. *ACS Photonics* **2018,** *5*, 3214-3221.

(7) Li, M.; Pernice, W.; Tang, H., Tunable Bipolar Optical Interactions between Guided Lightwaves. *Nat. Photonics* **2009,** *3*, 464-468.

(8) Roels, J.; Vlaminck, I. D.; Lagae, L.; Maes, B.; Thourhout, D. V.; Baets, R., Tunable Optical Forces between Nanophotonic Waveguides. *Nat. Nanotechnol.* **2009,** *4*, 510-513.

(9) Ren, M.; Huang, J.; Cai, H.; Tsai, J. M.; Zhou, J.; Liu, Z.; Suo, Z.; Liu, A.-Q., Nano-Optomechanical Actuator and Pull-Back Instability. *ACS Nano* **2013,** *7*, 1676-1681.

(10) Van Thourhout, D.; Roels, J., Optomechanical Device Actuation through the Optical Gradient Force. *Nat. Photonics* **2010,** *4*, 211-217.

(11) Eichenfield, M.; Michael, C. P.; Perahia, R.; Painter, O., Actuation of Micro-Optomechanical Systems Via Cavity-Enhanced Optical Dipole Forces. *Nat. Photonics* **2007,** *1*, 416-422.

(12) Bagheri, M.; Poot, M.; Li, M.; Pernice, W. P.; Tang, H. X., Dynamic Manipulation of Nanomechanical Resonators in the High-Amplitude Regime and Non-Volatile Mechanical Memory Operation. *Nat. Nanotechnol.* **2011,** *6*, 726-732.

(13) Ren, L.; Xu, X.; Zhu, S.; Shi, L.; Zhang, X., Experimental Realization of on-Chip Nonreciprocal Transmission by Using the Mechanical Kerr Effect. *ACS Photonics* **2020,** *7*, 2995-3002.

(14) Peng, B.; Özdemir, Ş. K.; Chen, W.; Nori, F.; Yang, L., What Is and What Is Not Electromagnetically Induced Transparency in Whispering-Gallery Microcavities. *Nat. Commun.* **2014,** *5*, 5082.

(15) Povinelli, M. L.; Johnson, S. G.; Lončar, M.; Ibanescu, M.; Smythe, E. J.; Capasso, F.; Joannopoulos, J., High-Q Enhancement of Attractive and Repulsive Optical Forces between Coupled Whispering-Gallery-Mode Resonators. *Opt. Express* **2005,** *13*, 8286-8295.

(16) Rakich, P. T.; Popović, M. A.; Soljačić, M.; Ippen, E. P., Trapping, Corralling and Spectral Bonding of Optical Resonances through Optically Induced Potentials. *Nat. Photonics* **2007,** *1*, 658-665.

(17) Deotare, P. B.; Bulu, I.; Frank, I. W.; Quan, Q.; Zhang, Y.; Ilic, R.; Loncar, M., All Optical Reconfiguration of Optomechanical Filters. *Nat. Commun.* **2012,** *3*, 846.

(18) Du, H.; Zhang, X.; Deng, J.; Zhao, Y.; Chau, F. S.; Zhou, G., Lateral Shearing Optical Gradient Force in Coupled Nanobeam Photonic Crystal Cavities. *Appl. Phys. Lett.* **2016,** *108*, 171102.

(19) Dong, B.; Cai, H.; Chin, L. K.; Huang, J. G.; Yang, Z. C.; Gu, Y. D.; Ng, G. I.; Ser, W.; Kwong, D. L.; Liu, A. Q., A Silicon-Nanowire Memory Driven by Optical Gradient Force Induced Bistability. *Appl. Phys. Lett.* **2015,** *107*, 261111.

(20) Cai, H.; Dong, B.; Tao, J.; Ding, L.; Tsai, J.; Lo, G.-Q.; Liu, A. Q.; Kwong, D. L., A Nanoelectromechanical Systems Optical Switch Driven by Optical Gradient Force. *Appl. Phys. Lett.* **2013,** *102*, 023103.

(21) Qiu, H.; Dong, J.; Liu, L.; Zhang, X., Energy-Efficient On-Chip Optical Diode Based on the Optomechanical Effect. *Opt. Express* **2017,** *25*, 8975-8985.

(22) Ciminelli, C.; Campanella, C. E.; Dell'Olio, F.; Armenise, M. N., Fast Light Generation through Velocity Manipulation in Two Vertically-Stacked Ring Resonators. *Opt. Express* **2010,** *18*, 2973-2986.

(23) Yariv, A., Universal Relations for Coupling of Optical Power between Microresonators and Dielectric Waveguides. *Electron. Lett.* **2000,** *36*, 321-322.

(24) Chuang, S. L., *Physics of Photonic Devices*. John Wiley & Sons, 2009.

(25) Haus, H. A.; Huang, W., Coupled-Mode Theory. *Proc. IEEE* **1991,** *79*, 1505-1518.

(26) Campanella, C. E.; Campanella, C. M.; De Leonardis, F.; Passaro, V. M. N., A High Efficiency Label-Free Photonic Biosensor Based on Vertically Stacked Ring Resonators. *The European Physical Journal Special Topics* **2014,** *223*, 2009-2021.

(27) Povinelli, M. L.; Lončar, M.; Ibanescu, M.; Smythe, E. J.; Johnson, S. G.; Capasso, F.; Joannopoulos, J. D., Evanescent-Wave Bonding between Optical Waveguides. *Opt. Lett.* **2005,** *30*, 3042-3044.

(28) Carmon, T.; Yang, L.; Vahala, K. J., Dynamical Thermal Behavior and Thermal Self-Stability of Microcavities. *Opt. Express* **2004,** *12*, 4742-4750.

(29) Xu, Q.; Lipson, M., Carrier-Induced Optical Bistability in Silicon Ring Resonators. *Opt. Lett.* **2006,** *31*, 341-343.

(30) Xu, M.; Wu, J.; Wang, T.; Hu, X.; Jiang, X.; Su, Y., Push–Pull Optical Nonreciprocal Transmission in Cascaded Silicon Microring Resonators. *IEEE Photonics J.* **2013,** *5*, 2200307.

(31) Barclay, P. E.; Srinivasan, K.; Painter, O., Nonlinear Response of Silicon Photonic Crystal Microresonators Excited Via an Integrated Waveguide and Fiber Taper. *Opt. Express* **2005,** *13*, 801-820.

(32) Zhang, Z.; Dainese, M.; Wosinski, L.; Qiu, M., Resonance-Splitting and Enhanced Notch Depth in SOI Ring Resonators with Mutual Mode Coupling. *Opt. Express* **2008,** *16*, 4621-4630.

(33) Li, Q.; Wang, T.; Su, Y.; Yan, M.; Qiu, M., Coupled Mode Theory Analysis of Mode-Splitting in Coupled Cavity System. *Opt. Express* **2010,** *18*, 8367-8382.

(34) Borselli, M.; Johnson, T. J.; Painter, O., Beyond the Rayleigh Scattering Limit in High-Q Silicon Microdisks: Theory and Experiment. *Opt. Express* **2005,** *13*, 1515-1530.

(35) Bogaerts, W.; De Heyn, P.; Van Vaerenbergh, T.; De Vos, K.; Selvaraja, S. K.; Claes, T.; Dumon, P.; Bienstman, P.; Van Thourhout, D.; Baets, R., Silicon Microring Resonators. *Laser Photonics Rev.* **2012,** *6*, 47-73.

(36) Xu, H.; Kemiktarak, U.; Fan, J.; Ragole, S.; Lawall, J.; Taylor, J. M., Observation of Optomechanical Buckling Transitions. *Nat. Commun.* **2017**, *8*, 14481.

(37) Grudinin, I. S.; Lee, H.; Painter, O.; Vahala, K. J., Phonon Laser Action in a Tunable Two-Level System. *Phys. Rev. Lett.* **2010,** *104*, 083901.

(38) Jing, H.; Özdemir, S. K.; Lü, X.-Y.; Zhang, J.; Yang, L.; Nori, F., PT-Symmetric Phonon Laser. *Phys. Rev. Lett.* **2014,** *113*, 053604.

(39) Jing, H.; Özdemir, Ş. K.; Geng, Z.; Zhang, J.; Lü, X.-Y.; Peng, B.; Yang, L.; Nori, F., Optomechanically-Induced Transparency in Parity-Time-Symmetric Microresonators. *Sci. Rep.* **2015,** *5*, 9663.

(40) Lu, T.-X.; Jiao, Y.-F.; Zhang, H.-L.; Saif, F.; Jing, H., Selective and Switchable Optical Amplification with Mechanical Driven Oscillators. *Phys. Rev. A* **2019,** *100*, 013813.

(41) Özdemir, Ş.; Rotter, S.; Nori, F.; Yang, L., Parity–Time Symmetry and Exceptional Points in Photonics. *Nat. Mater.* **2019,** *18*, 783-798.

(42) Miri, M.-A.; Alù, A., Exceptional Points in Optics and Photonics. *Science* **2019,** *363*, eaar7709.

(43) Thiruvenkatanathan, P.; Yan, J.; Woodhouse, J.; Seshia, A. A., Enhancing Parametric Sensitivity in Electrically Coupled Mems Resonators. *J. Microelectromech. Syst.* **2009,** *18*, 1077-1086.

For Table of Contents Use Only

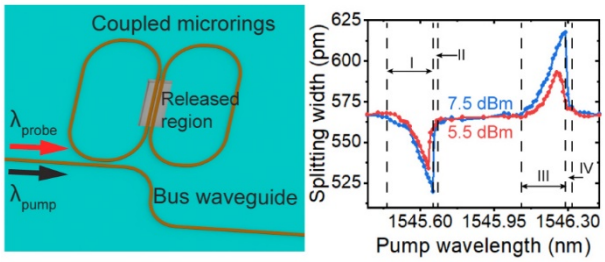

The left figure in the table of contents graphic contains a schematic of the optomechanical device based on two laterally coupled microrings. The right figure shows the measured splitting width between the S and AS resonances in the probe scan region when the pump wavelength is increased in the pump scan region.